Hindawi
Complexity
Volume 2024, Article ID 5594918, 15 pages
https://doi.org/10.1155/2024/5594918

Research Article

Cournot–Bertrand Duopoly Model: Dynamic Analysis Based on a Computed Cost

S. S. Askar and Ahmed M. Alshamrani

Department of Statistics and Operations Research College of Science, King Saud University, P.O. Box 2455, Riyadh 11451, Saudi Arabia

Correspondence should be addressed to S. S. Askar; saskar@ksu.edu.sa

Received 26 February 2023; Revised 19 September 2023; Accepted 18 January 2024; Published 6 February 2024

Academic Editor: Hiroki Sayama

In this paper, some mathematical properties and dynamic investigations of a Cournot–Bertrand duopoly game using a computed nonlinear cost are studied. The game is repeated and its evolution is presented by noninvertible map. The fixed points for this map are calculated and their stability conditions are discussed. One of those fixed points is Nash equilibrium, and the discussion shows that it can be unstable through flip and Neimark–Sacker bifurcation. The invariant manifold for the game's map is analyzed. Furthermore, the case when both competing firms are independent is investigated. Due to unsymmetrical structure of the game's map, global analysis gives rise to complicated basin of attraction for some attracting sets. The topological structure for these basins of attraction shows that escaping (infeasible) domain for some attracting sets becomes unconnected and the rise of holes is obtained. This confirms the existence of contact bifurcation.

1. Introduction

Cournot–Bertrand games have been analyzed and reported in several studies in the literature. They have been named after Cournot, the famous French economist, who first introduced duopoly games. Cournot work opened the route for many studies of the quantity competition between economic competitors. The current paper discusses a Cournot–Bertrand duopoly game based on a computed quantity cost. Cournot–Bertrand games take place when economic market contains two competitors producing the same type of commodity but with different strategies. These strategies are represented by quantity-setting and price-adjusting for achieving maximum profit.

The literature reported few studies on such games focusing on modelling the game and studying the Nash equilibrium point. For example, a simple Cournot duopoly model, which should actually be attributed to Bertrand, was considered in [1]. In [2], different cases of competitor's behaviors have been studied to show that the results developed in [3] are sensitive to the duopoly assumption. The work by Singh and Vives [3] was extended based on the asymmetry on cost and demand between competing firms in [4]. In [5], another extension of work of Singh and Vives [4] has been analyzed based on the role of outsourcing to a competitor. Based on a differentiation of production, Tremblay et al. [6] have modelled a Cournot–Bertrand game and have studied the stability condition of the game's Nash point in the static case. Askar in [7] has introduced a Cournot–Bertrand competition using three different mechanisms that are bounded rationality, best-reply reaction, and adaptive adjustment. In [7], the author proved that under certain conditions, the stability of Nash equilibrium point became asymptotically stable using the best-reply reaction and adaptive adjustment mechanism while bounded rationality method yielded a stable equilibrium point. Naimzada and Tramontana [8] studied some dynamic characteristics of Cournot–Bertrand game under differentiated products. They called two different mechanisms that are the best response and adaptive rule to build the game's model. They also compared their obtained results with results in the literature. In [9], other Cournot–Bertrand game

under certain market share has been established. That work has shown that the instability of Nash equilibrium point is obtained due to increase in the average utility. Other studies that have shown interesting results to those games and related games are reported in the literature such as Askar et al. [10–14], Wang and Ma [15], Ueda [16], Puu [17], Elsadany [18], Awad et al. [19], Zhou and Li [20], and Brianzani et al. [21]. For recent studies, the authors suggest the following works: Wei et al. [22] and Sarafopoulos and Papadopoulos [23].

The above studies have discussed different dynamic characteristics. Study of such dynamics often begins with the analysis of stability of the game equilibrium. Different types of bifurcations appear as a result of instability of the equilibrium point. They include period-doubling and Neimark–Sacker bifurcations. Important observations related the economic behavior of such games are detected due to deep investigation of attracting sets and chaotic behaviors of the games' discrete models. This also motivates searching for specific model dynamics and other phenomena such as synchronization, multistability, and contact bifurcation. Here one has to highlight important utility functions adopted in those games. There are several functions that have been the core in many studies such as the Cobb–Douglas function [8], constant elasticity of substitution or CES function [6], and Singh and Vives function [24]. The Cobb–Douglas one that is adopted here in this study has been intensively used because it has been formulated based on the technological constraints between the inputs and outputs of production. Furthermore, there have been certain mechanisms that have been adopted to estimate the behavior of firms (or economic competitors) such as naive rule [25], tit-for-tat method [26], local monopolistic approximation mechanism [27], and bounded rationality approach [28]. In this paper, we recall the bounded rationality approach to measure the competition between two firms. Our paper belongs to the above category of research direction but differs from them in which the cost function adopted by competing firms is not linear as many works in the literature have assumed. The firms' cost function in this game is computed based on Cobb–Douglas preference utility.

In this paper, we call the Cobb–Douglas utility function to evaluate the competitors' cost function. Based on certain economic constraints, a quadratic cost is used in the competition model. Using such cost with linear prices, the bounded rationality approach gives a nonlinear dynamic map describing the whole competition in discrete time periods. Our analysis shows that the model possesses three-corner fixed points and interior one representing Nash equilibrium. We use local and global analysis to investigate the stability of these points with intensive discussion on the basin of attraction due to the appearance of contact bifurcation under certain initial conditions.

In short, the current paper is organized as follows. In Section 2, the cost function is derived from the Cobb–Douglas function. The nonlinear discrete dynamic map describing the repetition of competition in discrete time periods with local analysis of its fixed points is given in Section 3. In Section 4, the invariant manifold is discussed. In some situations, the basin of attraction and global analysis around Nash point are investigated in Section 5. Finally, Section 6 discusses the obtained results.

2. Market Competition

Suppose a duopoly competition of two competing firms (or players) whose quantities are denoted by q_1 and q_2. Suppose also that the prices of those quantities are restricted as follows:

$$\begin{aligned} p_1 &= a - q_1 - \mathrm{d}q_2, \\ p_2 &= a - q_2 - \mathrm{d}q_1. \end{aligned} \tag{1}$$

The parameter $a > 0$ refers to a maximum price (in case there are no commodities sent to the market, i.e., $q_1 = q_2 = 0$). The parameter d denotes a degree of production whether it is a differentiation or substitution. In case of $d = 1$, the two competing players are identical and then homogeneous goods are raised while at $d = 0$, the two players are independent in prices and one gets a situation of two monopolistic players. When $d \in (0, 1)$, the competition turns into the case of substitutability. In this work, we study a mixed-type competition (or one can say a Cournot–Bertrand game). We assume that the first firm focuses on the quantity produced while the second firm puts its quantity's price forward as its decision variable. So, (1) can be rewritten in the form

$$\begin{aligned} p_1 &= a(1-d) - \left(1-d^2\right)q_1 + \mathrm{d}p_2, \\ q_2 &= a - p_2 - \mathrm{d}q_1. \end{aligned} \tag{2}$$

2.1. Computation of Cost and Profit Functions. According to the Cobb–Douglas utility, the quantities can be represented as follows [8]:

$$q_i = E_i L^{\alpha} K^{1-\alpha}; \quad i = 1, 2, \tag{3}$$

where $E_i, i = 1, 2$ denotes the total-factor productivity, L represents the total labor while the total capital is given by K, and α is taken as constant. For simplicity, we assume $\alpha = 0.5$. On the other hand, total cost can be given by

$$\mathrm{TC} = wL + rK, \tag{4}$$

where w and r refer to the wage per unit labor and the rental price per unit capital, respectively. From (3) and (4), one gets

$$\mathrm{TC}_i = \frac{wq_i^2}{E_i^2 K} + rK; \quad i = 1, 2, \tag{5}$$

while the marginal cost is given by $\mathrm{MC}_i = (dTC_i/dq_i) = c_i q_i; i = 1, 2$ and $c_i = (2w/E_i^2 K) > 0$. So, one can obtain the total profit of each firm as follows:

$$\pi_i = \mathrm{TR}_i - \mathrm{TC}_i; \quad i = 1, 2, \tag{6}$$

where the total revenue is given by $\mathrm{TR}_i = p_i q_i$. Now, (6) can be rewritten in the following form:

$$\pi_1 = \left[a(1-d) - \left(1-d^2\right)q_1 + \mathrm{d}p_2\right]q_1 - \frac{1}{2}c_1 q_1^2 - rK,$$
$$\pi_2 = (a - p_2 - \mathrm{d}q_1)p_2 - \frac{1}{2}c_2(a - p_2 - \mathrm{d}q_1)^2 - rK. \tag{7}$$

3. The Model

Studying the game's evolution requires recalling some production updating mechanisms which are used in forming discrete dynamic maps simulating this evolution. There are several mechanisms that have been reported in the literature, but in this paper, we recall the most popular one known as the bounded rationality mechanism. Such mechanism depends on the marginal profits, $(\eta_1 = (\partial\pi_1/\partial q_1), \eta_2 = (\partial\pi_2/\partial p_2))$, given by

$$\eta_1 = a(1-d) - \left(2 + c_1 - 2d^2\right)q_1 + \mathrm{d}p_2,$$
$$\eta_2 = a(1+c_2) - (2+c_2)p_2 - d(1+c_2)q_1. \tag{8}$$

Such marginal profits must be watched by firms for the production updating process. If both η_1 and η_2 are increasing, this means both profits are increasing and this encourages firms to increase their productions in the next time stage. For the case $\eta_1 > 0$ and $\eta_2 < 0$, only the first firm will increase its production while the second firm may leave competition and so the market. Similarly, the case $\eta_1 < 0$ and $\eta_2 > 0$ is clear. If $\eta_1 < 0$ and $\eta_2 < 0$, both firms may exit the competition. So, let us consider the case $\eta_1 > 0$ and $\eta_2 > 0$, and hence the updating process is given by

$$q_1(t+1) = q_1(t) + k_1 q_1 \eta_1,$$
$$p_2(t+1) = p_2(t) + k_2 p_2 \eta_2, \tag{9}$$

where $k_i > 0, i = 1, 2$ is called the speed of adjustment parameter. This means that both the relative production and price are directly proportional to η_1 and η_2, i.e., $q_1(t+1) - q_1(t)/q_1(t) \propto \eta_1$ and $p_2(t+1) - p_2(t)/p_2(t) \propto \eta_2$. Substituting (8) in (9), one gets the following map:

$$T(q_1, p_2): \begin{cases} q_1(t+1) = q_1(t) + k_1 q_1(t)\left[a(1-d) - \left(2 + c_1 - 2d^2\right)q_1(t) + dp_2(t)\right], \\ p_2(t+1) = p_2(t) + k_2 p_2(t)\left[a(1+c_2) - (2+c_2)p_2(t) - d(1+c_2)q_1(t)\right]. \end{cases} \tag{10}$$

It is a two-dimensional nonlinear discrete map and is used to simulate the game's repetition (or the game's evolution with respect to time t, $t = 0, 1, 2, \ldots$).

3.1. Fixed Points and Their Stability. At $q_1(t+1) = q_1(t)$ and $p_2(t+1) = p_2(t)$, map (10) admits four fixed points given by

$$O = (0, 0),$$
$$e_1 = \left(\frac{a(1-d)}{2 + c_1 - 2d^2}, 0\right),$$
$$e_2 = \left(0, \frac{a(1+c_2)}{2+c_2}\right),$$
$$e_* = \left(\frac{a(2+c_2-d)}{(2+c_1)(2+c_2) - (3+c_2)d^2}, \frac{a(1+c_2)\left(2+c_1-d-d^2\right)}{(2+c_1)(2+c_2) - (3+c_2)d^2}\right). \tag{11}$$

Since $a > 0, c_i > 0, i = 1, 2$, and $d \in (0, 1)$, simple calculations show that the above fixed points are positive. In addition, the points O, e_1, and e_2 imply that at least one firm will exit the market. Now, some propositions are obtained and their proofs are presented in Appendix.

Proposition 1. *The boundary $O = (0, 0)$ is unstable repelling node.*

Proposition 2. *The boundary e_1 is saddle point if $0 < k_1 < 2/a(1-d)$. Otherwise, it is an unstable node.*

Proposition 3. *The boundary e_2 is saddle point if $0 < k_2 < 2/a(1+c_2)$. Otherwise, it is an unstable node.*

Proposition 4. *The point e_* is known as Nash equilibrium point and is asymptotically stable if $0 < 1 - \delta < 4$ where δ is the determinant of Jacobian matrix at e_*.*

Proposition 5. *Due to flip bifurcation, Nash point becomes unstable if*

$$k_1 k_2 < \frac{k_1\left(2 + c_1 - 2d^2\right)}{a(1+c_2)(2 + c_1 - d(1+d))} + \frac{k_2(2+c_2)}{a(2+c_2-d)}. \quad (12)$$

Proposition 6. *Due to Neimark–Sacker bifurcation, the Nash point becomes unstable if*

$$k_1 k_2 > \frac{k_1\left(2 + c_1 - 2d^2\right)}{a(1+c_2)(2 + c_1 - d(1+d))} + \frac{k_2(2+c_2)}{a(2+c_2-d)}. \quad (13)$$

Figures 1(a)–1(c) show the region of stability for e_* at the values $a = 0.65, c_1 = 0.1, c_2 = 0.2$ and different values for d. It is clear that as d increases, the region of stability increases and vice versa. Numerical simulation shows also that any increase in a while the other parameters are fixed reduces the region of stability. Figure 1(d) presents the basin of attraction of the point e_* that is comprised of two regions, feasible and infeasible regions. More discussion on those regions will be given later in the Global Analysis section.

3.2. Critical Curves and Noninvertible Property. It is clear that map (10) belongs to the class C^1 (continuously differentiable). This means that the set LC_{-1} can be defined as follows:

$$\mathrm{LC}_{-1} \subseteq \left\{(q_1, p_2) \in \mathbb{R}^2 \colon \det\left(J(q_1, p_2)\right) = 0\right\}, \quad (14)$$

where $J(q_1, q_2)$ represents the Jacobian matrix which contains the locus of all points at which the determinant of Jacobian vanishes. The critical curves depend on this set and are used to give more information on the decision space of the map. Knowing those curves gives more information on the regions (or zones) dividing the decision space. The rank-1 of critical curves is denoted by LC and is defined as the locus of all rank-1 preimages located on the set LC_{-1}. So, LC represents all the rank-1 images of LC_{-1} under the map T given in (10), i.e., $\mathrm{LC} = T(\mathrm{LC}_{-1})$. For (10), LC_{-1} is given by

$$Aq_2^2 + Bp_1^2 + Cq_1p_2 - Dq_1 - Ep_2 + F = 0, \quad (15)$$

where

$$\begin{aligned}
A &= 2k_1k_2d(1+c_2)\left(2 + c_1 - 2d^2\right),\\
B &= -2k_1k_2d(2+c_2),\\
C &= 4k_1k_2(2+c_2)\left(2 + c_1 - 2d^2\right),\\
D &= -k_1k_2a(1+c_2)(4 + 2c_1 + d(1-5d)) - k_2d(1+c_2) - 2k_1\left(2 + c_1 - 2d^2\right),\\
E &= -k_1k_2a(4 + 2c_2 - d(5+3c_2)) - 2k_2(2+c_2) + dk_1,\\
F &= k_1k_2aa^2(1-d)(1+c_2) + k_2a(1+c_2) + k_1a(1-d) + 1.
\end{aligned} \quad (16)$$

Fixing the parameters values $a = 0.65, c_1 = 0.1, c_2 = 0.2, k_1 = 3.99, k_2 = 2.94$, and $d = 0.25, 0.50$, both LC_{-1} and LC are depicted in Figures 2(a)–2(d). At $d = 0.25$, it is obvious that $\mathrm{LC}_{-1} = \mathrm{LC}_{-1}^a \cup LC_{-1}^b$ and $\mathrm{LC} = \mathrm{LC}^a \cup \mathrm{LC}^b$ (as given in Figures 2(a) and 2(b)). One can see that the decision space of map (10) is divided into three zones known with Z_4, Z_2, and Z_0. Therefore, the map belongs to $Z_4 - Z_2 - Z_0$ type, and hence it is a noninvertible map. The shape of those zones is affected once an increase in the parameter d takes place (see Figures 2(c) and 2(d)).

Furthermore, from the structure of map (10), one can see that at $q_1(t) = 0$ or $p_2(t) = 0$, one gets $q_1(t+1) = 0$ or $p_2(t+1) = 0$ and this makes us to calculate the four real rank-1 preimages of the origin point. Putting $q_1(t+1) = 0$ and $p_2(t+1) = 0$ in (10) and solving the corresponding algebraic system, we get

$$\begin{aligned}
O &= (0, 0),\\
O_{-1}^{(1)} &= \left(\frac{1 + k_1a(1-d)}{k_1\left(2 + c_1 - 2d^2\right)}, 0\right),\\
O_{-1}^{(2)} &= \left(0, \frac{1 + k_2a(1+c_2)}{k_2(2+c_2)}\right),\\
O_{-1}^{(3)} &= \left(\frac{k_1ka(2+c_2-d)_2 + (2+c_2)k_2 + dk_1}{k_1k_2\left[(2+c_1)(2+c_2) - (3+c_2)d^2\right]}, \frac{k_1k_2a(1+c_2)(2+c_1-d(1+d)) - k_2d(1+c_1) + k_1\left(2+c_1-2d^2\right)}{k_1k_2\left[(2+c_1)(2+c_2) - (3+c_2)d^2\right]}\right).
\end{aligned} \quad (17)$$

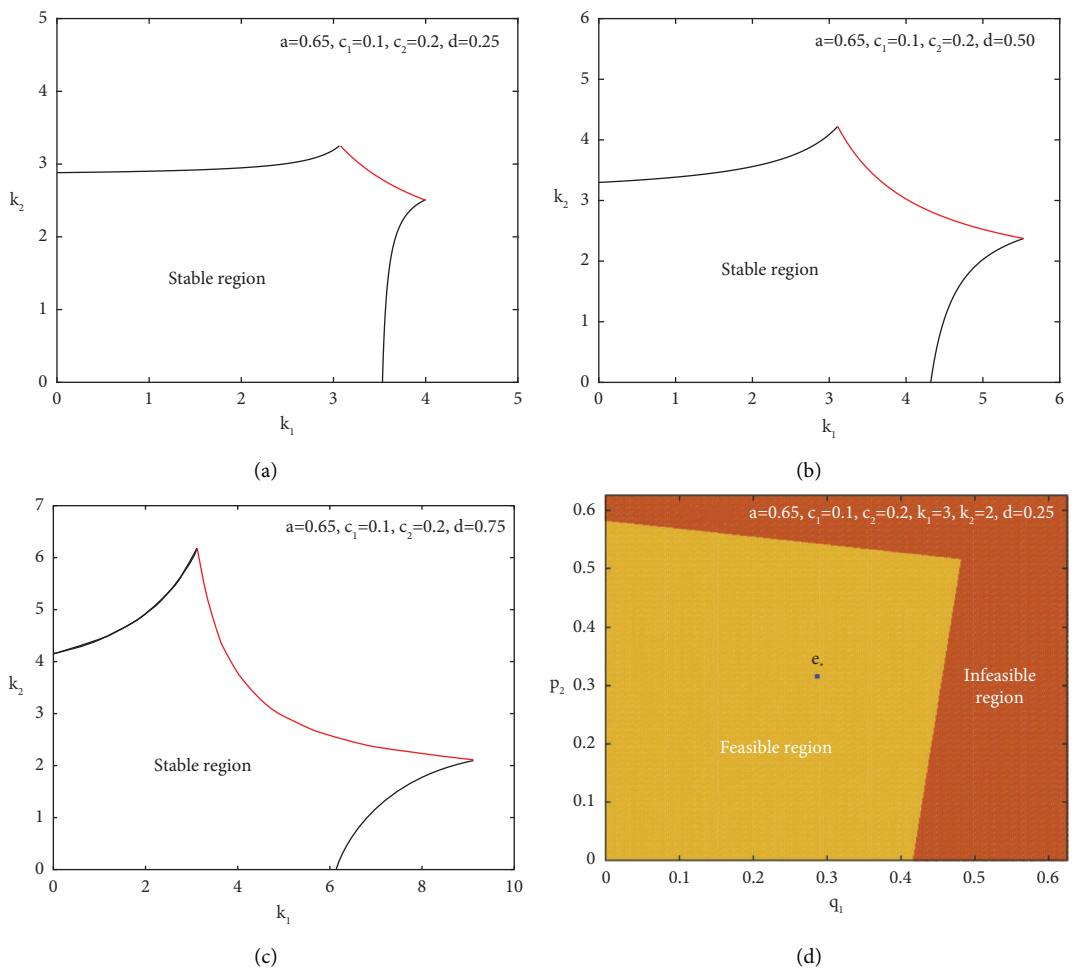

FIGURE 1: The region of stability for e_* at the values $a = 0.65, c_1 = 0.1, c_2 = 0.2$ and (a) $d = 0.25$. (b) $d = 0.50$. (c) $d = 0.75$. (d) The attractive basin of the equilibrium point e_* at the values, $k_1 = 3, k_2 = 2$ and $d = 0.25$. (a–c) The phase portrait for the stability region at different values of the parameter d while the other parameter values are fixed.

For convenience, let $w_1 = OO^1_{-1}$ and $w_2 = OO^2_{-1}$ represent two line segments on the invariant axes q_1 and p_2. Let w_1^{-1} and w_2^{-1} be their rank-1 preimages, respectively. So, for any points in the form $(q, 0) \in w_1$ and $(0, p) \in w_2$, their rank-1 preimages can satisfy the following algebraic systems:

$$\begin{cases} q = q_1 + k_1 q_1 \left[a(1-d) - \left(2 + c_1 - 2d^2\right)q_1 + d p_2\right], \\ 0 = p_2 + k_2 p_2 \left[a(1+c_2) - (2+c_2)p_2 - d(1+c_2)q_1\right], \end{cases}$$
$$\begin{cases} 0 = q_1 + k_1 q_1 \left[a(1-d) - \left(2 + c_1 - 2d^2\right)q_1 + d p_2\right], \\ p = p_2 + k_2 p_2 \left[a(1+c_2) - (2+c_2)p_2 - d(1+c_2)q_1\right]. \end{cases} \tag{18}$$

So, both w_1^{-1} and w_2^{-1} can be presented by

$$\begin{aligned} w_1^{-1}&: \ p_2 = 0 \text{ or } 1 + k_2\left[a(1+c_2) - (2+c_2)p_2 - d(1+c_2)q_1\right] = 0, \\ w_2^{-1}&: \ q_1 = 0 \text{ or } 1 + k_1\left[a(1-d) - \left(2 + c_1 - 2d^2\right)q_1 + d p_2\right] = 0. \end{aligned} \tag{19}$$

In Figure 3, those line segments are plotted at the values $a = 0.65, c_1 = 0.1, c_2 = 0.2, k_1 = 3.99, k_2 = 2.94$, and $d = 0.25$. They divide the phase plane into two regions known as feasible (orange color) and infeasible (light brown color) regions as shown in Figure 3. It is also clear that both w_1^{-1} and w_2^{-1} intersect in the point $O^{(3)}_{-1}$. Furthermore, the feasible region for any

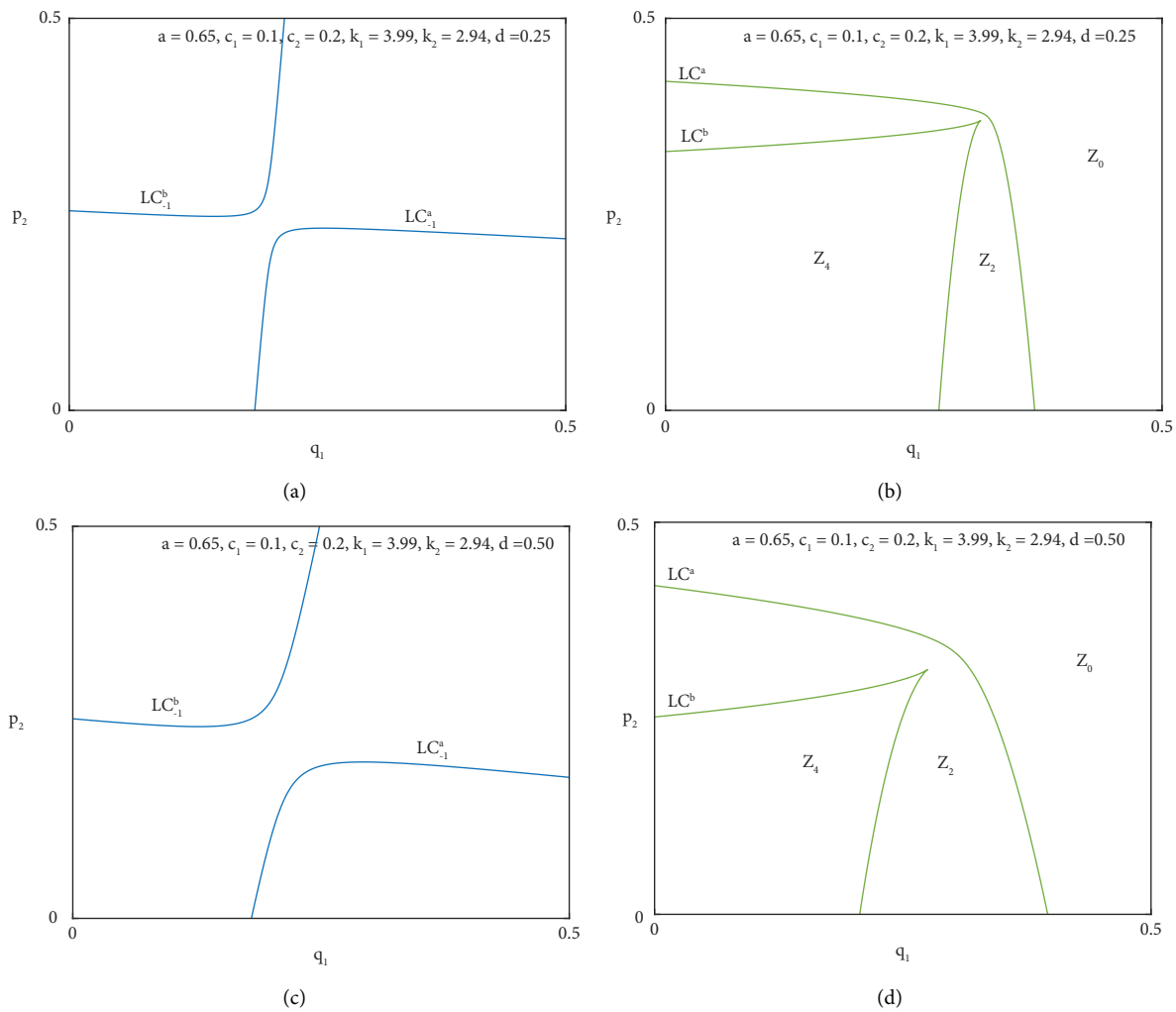

FIGURE 2: Both LC_{-1} and LC for map (10) at the parameters values $a = 0.65, c_1 = 0.1, c_2 = 0.2, k_1 = 3.99, k_2 = 2.94$. (a, b) $d = 0.25$. (c, d) $d = 0.50$.

attractor κ that may be Nash point, periodic cycle, or complex attractor will be bounded by a convex quadrilateral shape whose nodes are $O, O_{-1}^{(1)}, O_{-1}^{(2)}$, and $O_{-1}^{(3)}$.

3.3. Local Bifurcation. As one can see, the game's map (10) contains many parameters, but we focus here on the complex behavior that can be raised due to the change in k_1, k_2, and a. Both parameters k_1 and k_2 are known as speed of adjustments and most studies in the literature have concentrated on their influences on the time evolution of their games due to their economic meanings. In this section, we investigate the great change that may occur in the map's dynamics due to slight variations on those parameters. Those parameters are selected to be the principle cause of the types of bifurcations that may be raised. Let us begin with the following parameters values: $a = 0.65, c_1 = 0.1, c_2 = 0.2, d = 0.25$. It is clear in Figure 4(a) that when fixing $k_2 = 2$, the Nash point e_* becomes locally stable with respect to the speed parameter k_1 till this parameter reaches the value of period-2 cycle. As the parameter k_1 increases further, different types of periodic cycles such as period 4 and period 8 appeared. After period 8, higher period cycles appear, followed by chaos and then the point becomes unstable. Indeed, this type of bifurcation is called period-doubling (or flip) bifurcation and its Lyapunov exponent diagram is associated in this figure. Figure 4(b) shows the influence of the other speed parameter at the same parameters values but at $k_1 = 2$. It shows a flip bifurcation on varying the parameter k_2. In addition, simulation shows that the stability region with respect to the speed parameters is affected by the two parameters a and d. The simulation shows that as the parameter a increases, the stability region decreases and vice versa while as d increases, the region of stability increases and vice versa. For the dynamics of the map, another type of bifurcation is obtained. Let us keep the parameter values as previously but change $k_2 = 2.7$. As one can see, Figure 4(c) presents a stable Nash point that loses its stability through Neimark–Sacker (NS) bifurcation as k_1 increases. Figure 4(d) shows this type of bifurcation at the same values with respect to k_2 by fixing $k_1 = 3.2$. The same observation on the influences of the parameters a and d on this type of bifurcation is obtained. To end this subsection, Figure 4(e) shows the

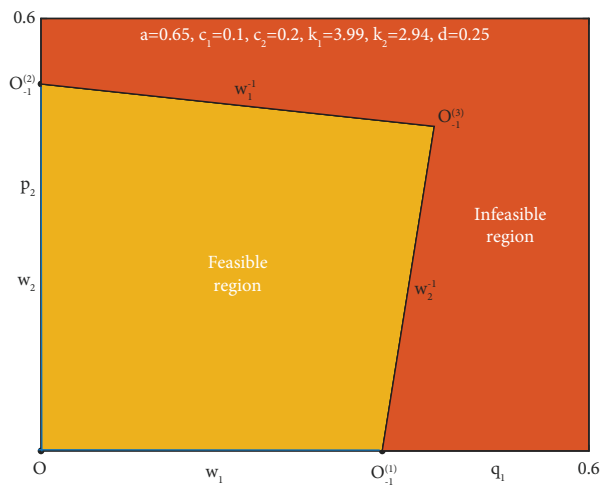

FIGURE 3: The line segments w_1 and w_2 and their preimages w_1^{-1} and w_2^{-1} at the parameters values $a = 0.65, c_1 = 0.1, c_2 = 0.2, k_1 = 3.99, k_2 = 2.94$, and $d = 0.25$.

influence of the parameter a on the map's dynamics when fixing the parameters to $c_1 = 0.1, c_2 = 0.2, d = 0.25, k_1 = 2$, and $k_2 = 2$. It shows that the Nash point becomes unstable due to NS-bifurcation.

To end this section, we discuss the codimension that occurs according to the above analysis. We recall standard software package MATCONT [29]. First, we can determine the curve of period-doubling bifurcations for the Nash point e_* by using one of the following PD points as initial point and adjusting the parameters k_1 and k_2 as free parameters.

The associated normal form coefficient of PD = $4.994128e + 01$.

The associated normal form coefficient of PD = $4.012625e + 01$.

Figure 4(f) displays the calculated PD curve. Notable features of the PD bifurcation curve include the fold-flip bifurcation (labeled as LPPD), the 1 : 2 resonance (labeled as $R2$), and the generalized flip bifurcation (labeled as GPD). The MATCONTM outputs are reported as follows.

label = LPPD, $x = (q_1, q_2, k_1, k_2) = (0.286765, 0.315441, 3.531321, 0.000000)$.

Normal form coefficient for LPPD: $[a/e, be] = [4.118997e - 09, -4.733743e - 10]$.

label = $R2, x = (0.286765, 0.315441, 3.991320, 2.506554)$.

Normal form coefficient for $R2$: $[c, d] = [-8.674046e + 00, -2.515713e + 02]$.

label = GPD, $x = (0.286765, 0.315441, 4.043296, 2.536229)$.

Normal form coefficient of GPD = $-2.943603e + 04$.

Second, we conduct the Neimark–Sacker bifurcation curve for the Nash point e_*.

By picking up one of the following NS points as initial point and varying k_1 and k_2 as free parameters.

The associated normal form coefficient of NS = $-6.219393e + 01$.

The associated normal form coefficient of NS = $-6.528657e + 01$.

The associated normal form coefficient of NS = $-2.658829e + 01$.

Figure 4(g) depicts the calculated NS curve. The label $R2$ refers to the 1: 2 resonance on the Neimark–Sacker bifurcation curve. The MATCONTM outputs are reported as follows.

label = $R2, x = (0.286765, 0.315441, 3.071322, 3.257379)$.

Normal form coefficient of $R2$: $[c, d] = [2.610720e + 00, -2.704883e + 02]$.

label = $R2, x = (0.2867650.3154413.9913202.506554)$.

Normal form coefficient of $R2$: $[c, d] = [-8.665654e + 00, -2.515804e + 02]$.

4. The Invariant Manifold

Initiating map (10) at the initial state $q_1(t) = 0$ or $p_2(t) = 0$ makes it getting trapped to the point (0, 0). That is to say, if $q_1(t) = 0$ or $p_2(t) = 0$, then $q_1(t+1) = 0$ or $p_2(t+1) = 0$ and then the axes $\overrightarrow{Oq_1}$ and $\overrightarrow{Op_2}$ become invariant axes. Those invariant axes will form an invariant manifold for map (10) and then its dynamics will be governed by one of the following one-dimensional maps:

$$q_1(t+1) = [1 + k_1 a(1-d)]\, q_1(t)\left(1 - \frac{k_1\left(2 + c_1 - 2d^2\right)}{1 + k_1 a(1-d)} q_1(t)\right), \tag{20}$$

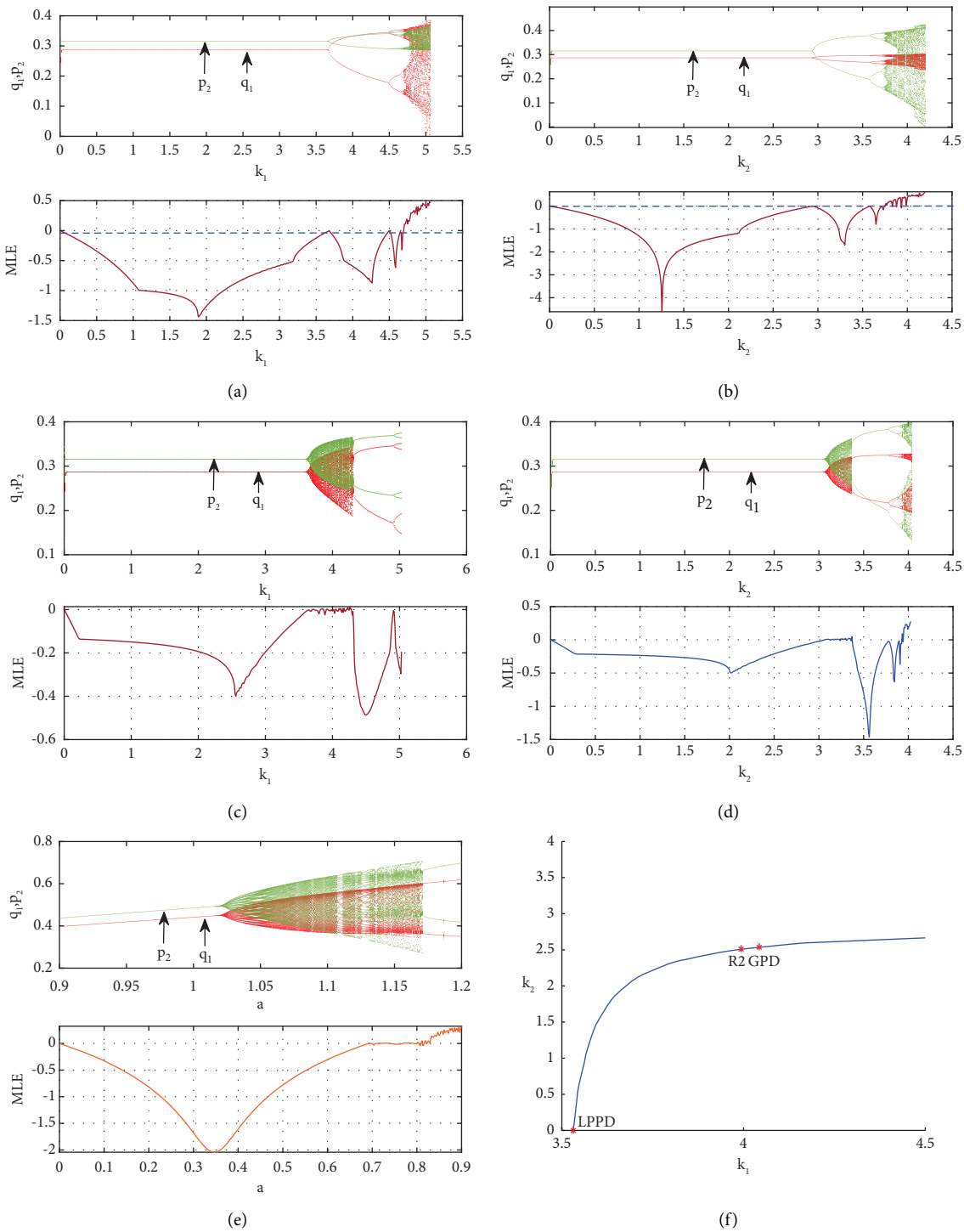

Figure 4: Continued.

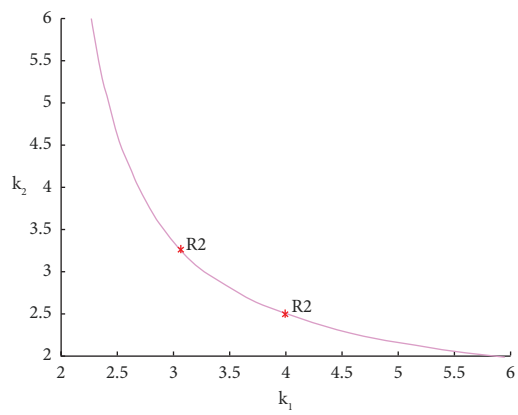

(g)

Figure 4: The bifurcation diagrams at $a = 0.65, c_1 = 0.1, c_2 = 0.2, d = 0.25$, and (a) on varying k_1 with $k_2 = 2$. (b) On varying k_2 with $k_1 = 2$. (c) On varying k_1 with $k_2 = 2.7$. (d) On varying k_2 with $k_1 = 3.2$. (e) The influence of the parameter a on the dynamics of map (9) at the values, $c_1 = 0.1, c_2 = 0.2, d = 0.25, k_1 = 2$ and $k_2 = 2$. (f) Period doubling bifurcation curve with Fold-Flip bifurcation (LPPD), 1 : 2 resonance ($R2$), and generalized flip bifurcation (GPD) are centered on the PD point. (g) The 1: 2 resonance ($R2$) comprises the majority of the Neimark–Sacker bifurcation curve.

or

$$p_2(t+1) = [1 + k_2 a(1+c_2)]\, p_2(t)\left(1 - \frac{k_2(2+c_2)}{1+k_2 a(1+c_2)} p_2(t)\right), \tag{21}$$

which can be rewritten in the following forms:

$$\begin{aligned} x(t+1) &= \mu_1 x(t)(1 - x(t)), \\ y(t+1) &= \mu_2 y(t)(1 - y(t)), \end{aligned} \tag{22}$$

where

$$\begin{aligned} \mu_1 &= 1 + k_1 a(1-d), \\ \mu_2 &= k_2 a(1+c_2), \\ q_1(t) &= \frac{1 + k_1 a(1-d)}{k_1\left(2 + c_1 - 2d^2\right)} x(t), \\ p_2(t) &= \frac{1 + k_2 a(1+c_2)}{k_2(2+c_2)} y(t). \end{aligned} \tag{23}$$

The linear transformation given in (23) makes both (20) and (21) topologically equivalent to the well-known logistic map.

4.1. Dynamic Analysis. Let us discuss the complex dynamics of the one-dimensional map (20). This map possesses two fixed points that are $\overline{q}_1 = 0$ and $\overline{q}_1 = a(1-d)/2 + c_1 - 2d^2$. Simple calculations show that $|dq_1(t+1)/dq_1(t)|_{\overline{q}_1=0} = |1 + k_1 a(1-d)| > 1$ and hence $\overline{q}_1 = 0$ becomes unstable node. For the second fixed point, one gets $|dq_1(t+1)/dq_1(t)| = |1 - k_1 a(1-d)|$ which is stable if $k_1 < 2/a(1-d)$. If $k_1 = k_f = 2/a(1-d)$, a period-doubling bifurcation emerges. This means that at the critical value $k_1 = 2/a(1-d)$, the trajectories of map (20) commencing on the invariant axis $\overrightarrow{Oq_1}$ diverge when $k_1 \in (2/a(1-d), +\infty)$. Furthermore, the preimages of $q_1(t+1) = 0$ are 0 and $q = 1 + k_1 a(1-d)/k_1(2 + c_1 - 2d^2)$ which means it belongs to Z_2 zone. Any point q_1 such that $q_1 > q$ will have no preimages and therefore map (20) will belong to $Z_2 - Z_0$ type. The same discussion is for map (21). It has two fixed points, $\overline{p}_2 = 0$ and $\overline{p}_2 = a(1+c_2)/2 + c_2$. The point $\overline{p}_2 = 0$ is unstable node since $|dp_2(t+1)/dp_2(t)|_{p_2=0} = |1 + k_2 a(1+c_2)| > 1$. At the other point, one gets $|dp_2(t+1)/dp_2(t)| = |1 - k_2 a(1+c_2)|$ and hence it is stable if $k_2 < 2/a(1+c_2)$. If $k_2 = k_f = 2/a(1+c_2)$, a period-doubling bifurcation emerges. This means that at the critical value $k_2 = 2/a(1+c_2)$, the trajectories of map (21) commencing on the invariant axis $\overrightarrow{Op_2}$ diverge when $k_2 \in (2/a(1+c_2), +\infty)$. The preimages of $p_2(t+1) = 0$ are 0 and $p = 1 + k_2 a(1+c_2)/k_2(2+c_2)$ which means it belongs to Z_2 zone. Any point p_2 such that $p_2 > p$ will have no preimages and therefore map (21) will belong to $Z_2 - Z_0$ type. Figures 5(a) and 5(b) show a simulation of chaotic attractors for maps (20) and (21) at the parameters values, $a = 0.65, c_1 = 0.1, k_1 = 6.1, d = 0.25$ for Figure 5(a) and $a = 0.65, c_2 = 0.2, k_2 = 3.83$ for Figure 5(b). As one can see, the feasible regions are bounded by $[0, q] \times [0, q]$ and $[0, p] \times [0, p]$ that separate Z_2 and Z_0 zones. The orange color denotes diverging points belonging to the infeasible region.

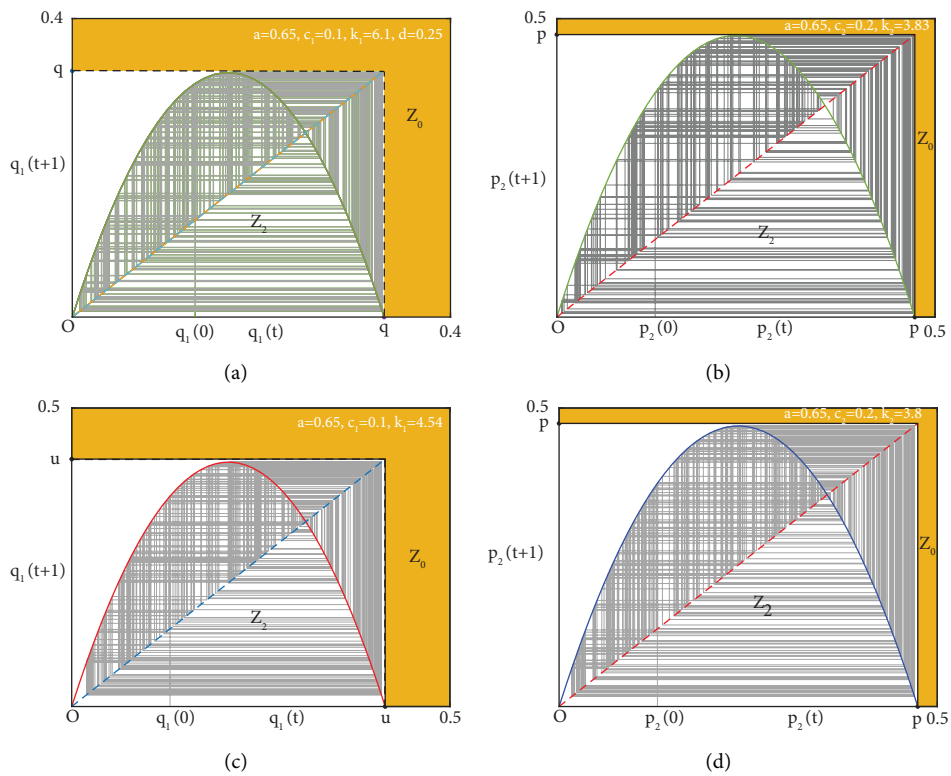

FIGURE 5: Chaotic situation for the maps (20) and (21) occurred at the parameters values (a) $a = 0.65, c_1 = 0.1, k_1 = 6.1, d = 0.25$ and (b) $a = 0.65, c_2 = 0.2, k_2 = 3.83$. Chaotic situation for each part of the map (24) occurred at the parameters values (c) $a = 0.65, c_1 = 0.1, k_1 = 4.54$ and (d) $a = 0.65, c_2 = 0.2, k_2 = 3.8$.

4.2. Independent Firms. At $d = 0$, map (10) is reduced to two monopolistic firms with independent products. It becomes as follows:

$$T(d=0): \begin{cases} q_1(t+1) = q_1(t) + k_1 q_1(t)\left[a - (2+c_1)q_1(t)\right], \\ p_2(t+1) = p_2(t) + k_2 p_2(t)\left[a(1+c_2) - (2+c_2)p_2(t)\right]. \end{cases} \tag{24}$$

Each part in map (24) conjugates the logistic map, $z_i(t+1) = v_i z(t)(1 - z(t)), i = 1, 2$ and $v_1 = 1 + ka$ and $v_2 = 1 + k_2 a(1 + c_2)$. The same discussion and analysis for each part in map (24) can be carried out as above but we here give a simulation for two chaotic attractors for (24). The preimages of $q_1(t+1) = 0$ are 0 and $u = 1 + k_1 a/k_1(2 + c_1)$. The preimages of $p_2(t+1) = 0$ are 0 and p. Figures 5(c) and 5(d) show a simulation of chaotic attractors for each part in map (24) at the parameters values, $a = 0.65, c_1 = 0.1, k_1 = 4.54$ for Figure 5(c) and $a = 0.65, c_2 = 0.2, k_2 = 3.8$ for Figure 5(d). As one can see, the feasible regions are bounded by $[0, u] \times [0, u]$ and $[0, p] \times [0, p]$ that separate Z_2 and Z_0 zones. The orange color denotes diverging points belonging to the infeasible region.

5. Basin of Attraction and Global Analysis

Let us suppose that H is an attractor for map (10). The attractor H may represent Nash point, periodic cycle, or other complex attractor. The basin of attraction of H possesses all points forming bounded trajectories converging to H and is defined as

$$B(H) = \left\{(q_1, q_2) \in \mathbb{R}_+^2 : T^n(q_1, q_2) \longrightarrow H, n \longrightarrow \infty\right\}. \tag{25}$$

Suppose there is a neighborhood $\Omega(H)$ of the attractor H such that $\Omega(H) \subset B(H)$; then, one can represent $B(H)$ as $B(H) = \cup_{t=0}^{\infty} T^{-n}(\Omega(H))$. For a topological structure, the phase space map is divided into two regions, the feasible and infeasible regions. The feasible region possesses points with bounded trajectories and is formed by the attractive basin of all existing attractors. It is denoted by the closure set $F = \cup_{k=1}^{n} B(H_k)$. The infeasible region possesses points with unbounded (or divergent) trajectories and is denoted by $B(\infty)$. Both the boundaries of F and $B(\infty)$ denoted by $\partial B(F)$ and $\partial B(\infty)$, respectively, separate F from $B(\infty)$ and vice versa. So, we have $\partial B(F) = \partial B(\infty) = \partial B$ which is called the boundary of basin. For map (10), this boundary is defined by

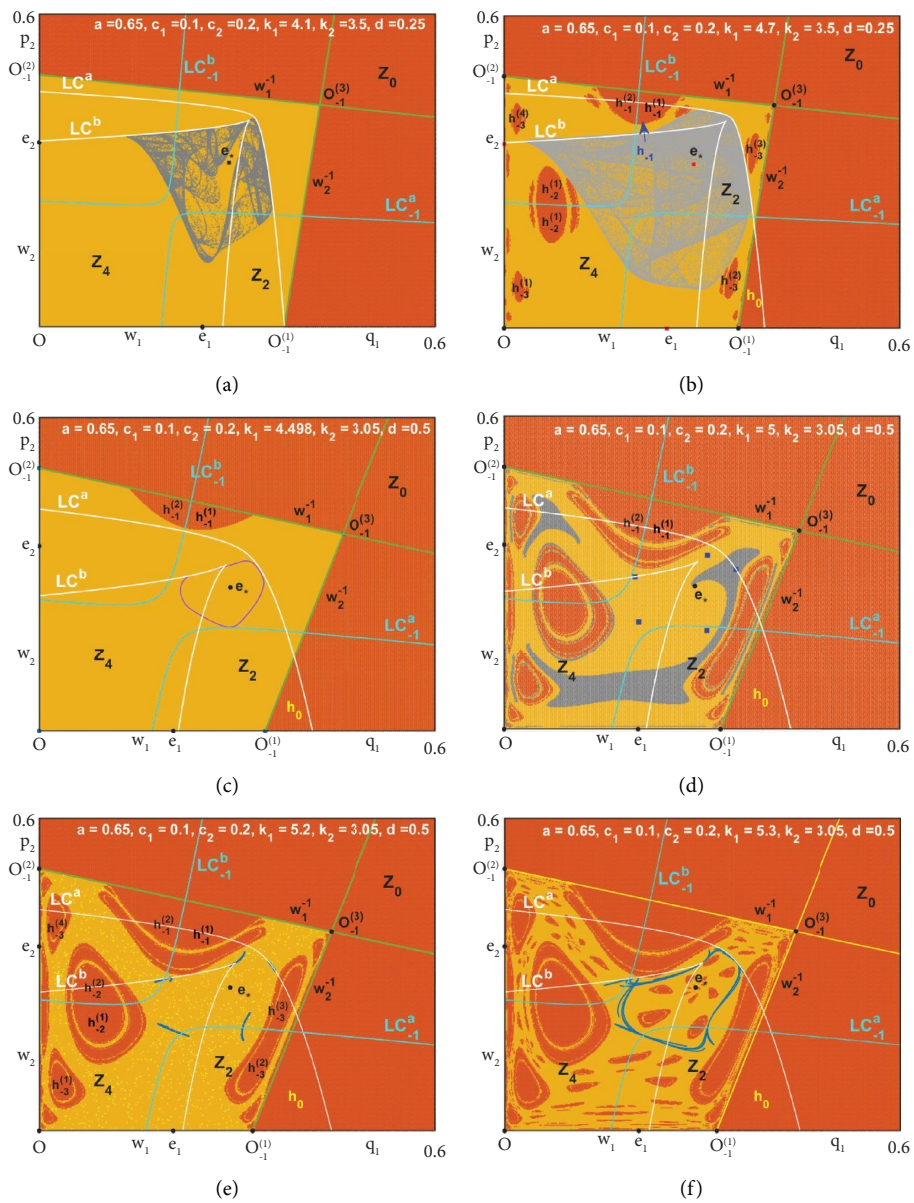

FIGURE 6: The basin of attraction of chaotic attractor at the values $(a, c_1, c_2, d, k_2) = (0.65, 0.1, 0.2, 0.25, 3.5)$ and (a) $k_1 = 4.1$, (b) $k_1 = 4.7$. For $(a, c_1, c_2, d, k_2) = (0.65, 0.1, 0.2, 0.5, 3.05)$ the basin of attraction of (c) a ring at $k_1 = 4.498$, (d) a period-5 cycle at $k_1 = 5$, (e) a five-bands chaotic attractor at $k_1 = 5.28$, (f) a chaotic attractor at $k_1 = 5.3$.

$$\partial B = \left(\bigcup_{n=0}^{\infty} T^{-n}(w_1)\right) \cup \left(\bigcup_{n=0}^{\infty} T^{-n}(w_2)\right). \tag{26}$$

In Figure 3, the basin of attraction of Nash point is plotted. As one can see, both w_1^{-1} and w_2^{-1} separate $B(E_*)$ colored by orange from $B(\infty)$ colored by brown. It is also clear that the basin of infeasible region is connected. So, in the next subsection, more details about the topological structure of the basin of attraction are discussed.

5.1. Global Analysis. Global analysis gives more information about the complex characteristics of an attractor H. It provides some topological structures regarding the basin of attraction of such attractor. These structures do not appear when performing local analysis on map (10) through changes in the map's parameters. This requires to investigate the qualitative changes occurring in these topological structure in the long term due to initial conditions taken far away from the map's equilibrium point. Let us assume the following parameters values: $(a, c_1, c_2, d, k_1, k_2) = (0.65, 0.1, 0.2, 0.25, 4.1, 3.5)$. Figure 6(a) shows a chaotic attractor born based on these values. As one can see, it presents a chaotic attractor (gray color) whose basin of attraction is represented by two colors (orange and brown). The feasible region is represented by orange and is bounded by the quadrilateral shape whose vertices are $O, O_{-1}^{(1)}, O_{-1}^{(2)}$, and $O_{-1}^{(3)}$, while the infeasible region (or the escaping domain) is plotted by brown. Furthermore, the escaping domain forms

a connected set and hence there is no sign of the appearance of contact bifurcation. The nonexistence of contact bifurcation is due to the fact there is no contact between the branch LC^a and the boundary line w_2^{-1}. Keeping the parameters values fixed and increasing k_1 to 4.7, the chaotic attractor becomes more complex and contact bifurcation takes place due to the appearance of the region h_0 between the branch LC^a and the boundary line w_2^{-1}. It is clear in Figure 6(b) that the region h_0 enters from Z_0 into Z_2 zone and hence the escaping domain will become a disconnected set. That is to say, each point in h_0 will possess two distinct real rank-1 preimages. Because of the disconnection of escaping domain, some holes are born in the feasible region. Each point belonging to h_0 possesses two preimages of rank-1 that are used to form the main hole h_{-1}. This main hole consists of two parts $h_{-1}^{(1)}$ and $h_{-1}^{(2)}$ that are connected by the branch LC_{-1}^b. It is clear from Figure 6(b) that the points of the main hole belong to two different zones that are Z_2 and Z_0. The points belonging to Z_2 have two distinct real rank-2 preimages and are used to construct the hole whose two parts are $h_{-2}^{(1)}$ and $h_{-2}^{(2)}$ which are entirely in Z_4 zone and are used to form the other small holes in the feasible regions $h_{-3}^{(1)}$, $h_{-3}^{(2)}, h_{-3}^{(3)}$, and $h_{-3}^{(4)}$.

Let us assume the following parameters values, $(a, c_1, c_2, d, k_1, k_2) = (0.65, 0.1, 0.2, 4.498, 3.05)$ but $d = 0.5$. Figure 6(c) shows that at these values, a closed ring is born due to Neimark–Sacker bifurcation. The basin of attraction of this ring shows also the appearance of main hole due to the region h_0 obtained as a result of contact bifurcation. Keeping the values fixed and increasing k_1, numerical simulation confirms this closed ring till $k_1 = 5$ where period-5 cycle emerges. Figure 6(d) presents the basin of attraction of this period cycle. As one can see, region h_0 gets larger and the number of holes increases. At $k_1 = 5.2$, this period cycle turns into a five-band chaotic attractor whose attractive basin is given in Figure 6(e). Further increase in k_1 to 5.3 gives a chaotic attractor with complicated basin of attraction full of many holes (see Figure 6(f)). Economically, the appearance of such complicated structures of basin of attractions makes the future evolution of game hard to predict if competing firms take initial states belonging to those holes.

6. Conclusion

This paper has presented a dynamic view for a Cournot–Bertrand duopoly game based on a computed nonlinear cost function derived from Cobb–Douglas utility. As in related studies in the literature, the fixed points for the game's map have been obtained and their stabilities using eigenvalues and Jury conditions have been discussed. The discussion has shown through local analysis that the Nash equilibrium point can be unstable due to flip and Neimark–Sacker bifurcation. Furthermore, we have found that when the competing firms have increased the parameter of degree of production, the region of stability becomes larger with respect to the speed parameters.

The global analysis of map has shown some complicated basin of attraction of some attracting sets. The noninvertible phenomena of the map and its critical curves have shown that its phase plane has been divided into three regions Z_0, Z_2, and Z_4. The basin of attraction of some attracting sets under certain parameters' value has shown the existence of holes from the escaping domain. These obtained holes are the preimages of the area of intersection formed by the critical curves, the boundary of the basin, and the invariant axis. Such raising holes are due to the existence of contact bifurcation, and as these holes increase, the future prediction of the game evolution becomes impossible if competing firms select initial states from those holes.

Appendix

The Jacobian matrix of map (10) becomes

$$J(q_1, p_2) = \begin{pmatrix} j_{11} & k_1 d q_1 \\ -(1+c_2)k_2 d p_2 & j_{22} \end{pmatrix}, \tag{A.1}$$

where

$$\begin{aligned} j_{11} &= 1 + k_1\left[a(1-d) - 2\left(2 + c_1 - 2d^2\right)q_1 + d p_2\right], \\ j_{22} &= 1 + k_2\left[a(1+c_2) - 2(2+c_2)p_2 - d(1+c_2)q_1\right]. \end{aligned} \tag{A.2}$$

Proof 1. At O, one gets

$$J(O) = \begin{bmatrix} 1 + k_1 a(1-d), & 0, \\ 0, & 1 + k_2 a(1+c_2). \end{bmatrix}. \tag{A.3}$$

The above matrix represents a diagonal matrix with two eigenvalues, $\lambda_1 = 1 + k_1 a(1-d)$ and $\lambda_2 = 1 + k_2 a(1+c_2)$ with eigenvectors (1,0) and (0, 1). It is simple to check that $|\lambda_i| > 1, i = 1, 2$ and then O is unstable repelling node.

Proof 2. At e_1, one gets

$$J(e_1) = \begin{bmatrix} 1 - k_1 a(1-d), & \dfrac{k_1 a d(1-d)}{2 + c_1 - 2d^2}, \\ 0, & 1 + \dfrac{k_2 a(1+c_2)(2 + c_1 - d(1+d))}{2 + c_1 - 2d^2}. \end{bmatrix}. \tag{A.4}$$

As one can see, matrix (A.4) is an upper triangular whose eigenvalues become

$$\lambda_1 = 1 - k_1 a(1-d),$$
$$\lambda_2 = 1 + \frac{k_2 a(1+c_2)(2+c_1-d(1+d))}{2+c_1-2d^2}, \tag{A.5}$$

with corresponding eigenvectors given by

$$\vec{\lambda}_1 = (1, 0),$$
$$\vec{\lambda}_2 = \left(1, \frac{k_1 d(1-d)}{k_2(1-d)\left(2+c_1-2d^2\right) + k_2(1+c_2)(2+c_1-d(1+d))}\right). \tag{A.6}$$

It is clear that $|\lambda_2| > 1$ for all auxiliary parameters and $|\lambda_1| < 1$ gives $0 < k_1 < 2/a(1-d)$ which means that e_1 is a saddle point. In case $k_1 > 2/a(1-d)$, then e_1 becomes an unstable node.

Proof 3. The proof is similar to Proposition 2.

Proof 4. At e_*, one gets

$$J(E_*) = \begin{bmatrix} \ell_{11} & \ell_{12} \\ \ell_{21} & \ell_{22} \end{bmatrix}, \tag{A.7}$$

where

$$\ell_{11} = 1 - \frac{k_1 a(2+c_2-d)\left(2+c_1-2d^2\right)}{4+2c_1-3d^2+c_2\left(2+c_1-d^2\right)},$$
$$\ell_{12} = \frac{k_1 ad(2+c_2-d)}{4+2c_1-3d^2+c_2\left(2+c_1-d^2\right)},$$
$$\ell_{21} = -\frac{k_2 ad(1+c_2)^2(2+c_1-d(1+d))}{4+2c_1-3d^2+c_2\left(2+c_1-d^2\right)},$$
$$\ell_{22} = 1 - \frac{k_2 a(1+c_2)(2+c_2)(2+c_1-d(1+d))}{4+2c_1-3d^2+c_2\left(2+c_1-d^2\right)}, \tag{A.8}$$

and then the trace τ and determinant δ take the following forms:

$$\tau = 2 - \frac{k_1 a(2+c_2-d)\left(2+c_1-2d^2\right)}{4+2c_1-3d^2+c_2\left(2+c_1-d^2\right)} - \frac{k_2 a(1+c_2)(2+c_2)(2+c_1-d(1+d))}{4+2c_1-3d^2+c_2\left(2+c_1-d^2\right)},$$
$$\delta = 1 - \frac{k_1 a(2+c_2-d)\left(2+c_1-2d^2\right)}{(2+c_1)(2+c_2)-(3+c_2)d^2} - \frac{k_2 a(1+c_2)(2+c_2)(2+c_1-d(1+d))}{(2+c_1)(2+c_2)-(3+c_2)d^2}$$
$$+ \frac{k_1 k_2 a^2((1+c_2)(2+c_2-d)(2+c_1-d(1+d)))}{(2+c_1)(2+c_2)-(3+c_2)d^2}. \tag{A.9}$$

Now the Jury conditions [10] can be calculated as follows:

$$1-\tau+\delta=\frac{k_1k_2a^2\left(2+c_2-d\right)\left(2+c_1-d\left(d+1\right)\right)}{4+2c_1-3d^2+c_2\left(2+c_1-d^2\right)}, \tag{A.10a}$$

$$\begin{aligned}1+\tau+\delta=4&-\frac{2k_1a\left(2+c_2-d\right)\left(2+c_1-2d^2\right)}{4+2c_1-3d^2+c_2\left(2+c_1-d^2\right)}-\frac{2k_2a\left(1+c_2\right)\left(2+c_2\right)\left(2+c_1-d\left(1+d\right)\right)}{4+2c_1-3d^2+c_2\left(2+c_1-d^2\right)}+\\&+\frac{k_1k_2a^2\left(1+c_2\right)\left(2+c_2-d\right)\left(2+c_1-d\left(1+d\right)\right)}{4+2c_1-3d^2+c_2\left(2+c_1-d^2\right)},\end{aligned} \tag{A.10b}$$

$$\begin{aligned}1-\delta=&-\frac{k_1k_2a^2\left(1+c_2\right)\left(2+c_2-d\right)\left(2+c_1-d\left(1+d\right)\right)}{4+2c_1-3d^2+c_2\left(2+c_1-d^2\right)}+\frac{k_1a\left(2+c_2-d\right)\left(2+c_1-2d^2\right)}{4+2c_1-3d^2+c_2\left(2+c_1-d^2\right)}+\\&+\frac{k_2a\left(1+c_2\right)\left(2+c_2\right)\left(2+c_1-d\left(1+d\right)\right)}{4+2c_1-3d^2+c_2\left(2+c_1-d^2\right)}.\end{aligned} \tag{A.10c}$$

Simple calculations show that condition (A.10a) is always positive. The point e^* becomes asymptotically stable if the conditions (A.10b) and (A.10c) are nonnegative. Combining those two conditions gives

$$0<1-\delta<4. \tag{A.11}$$

Proof 5. Suppose that condition (A.10b) is nonpositive and condition (A.10c) is kept nonnegative; then, combining those conditions gives

$$k_1k_2<\frac{k_1\left(2+c_1-2d^2\right)}{a\left(1+c_2\right)\left(2+c_1-d\left(1+d\right)\right)}+\frac{k_2\left(2+c_2\right)}{a\left(2+c_2-d\right)}. \tag{A.12}$$

Proof 6. Suppose that condition (A.10b) is nonnegative and condition (A.10c) is kept nonpositive; then, combining those conditions gives

$$k_1k_2>\frac{k_1\left(2+c_1-2d^2\right)}{a\left(1+c_2\right)\left(2+c_1-d\left(1+d\right)\right)}+\frac{k_2\left(2+c_2\right)}{a\left(2+c_2-d\right)}. \tag{A.13}$$

Data Availability

Data are included within the article.

Conflicts of Interest

The authors declare that they have no conflicts of interest.

Acknowledgments

This study was supported by the Researchers Supporting Project (RSP2024R167), King Saud University, Riyadh, Saudi Arabia.

References

[1] S. Bylka and J. Komar, "Cournot-Bertrand mixed oligopolies," in *Warsaw Fall Seminars in Mathematical Economics 1975*, M. Ło ś, J. Łoś, and A. Wieczorek, Eds., Springer, Berlin, Heidelberg, 1976.

[2] J. Häckner, "A note on price and quantity competition in differentiated oligopolies," *Journal of Economic Theory*, vol. 93, no. 2, pp. 233–239, 2000.

[3] N. Singh and X. Vives, "Price and quantity competition in a differentiated duopoly," *The RAND Journal of Economics*, vol. 15, no. 4, pp. 546–554, 1984.

[4] P. Zanchettin, "Differentiated duopoly with asymmetric costs," *Journal of Economics and Management Strategy*, vol. 15, no. 4, pp. 999–1015, 2006.

[5] A. Arya, B. Mittendorf, and D. E. M. Sappington, "Outsourcing, vertical integration, and price vs. quantity competition," *International Journal of Industrial Organization*, vol. 26, no. 1, pp. 1–16, 2008.

[6] C. H. Tremblay and V. J. Tremblay, "The Cournot-Bertrand model and the degree of product differentiation," *Economics Letters*, vol. 111, no. 3, pp. 233–235, 2011.

[7] S. S. Askar, "On Cournot–Bertrand competition with differentiated products," *Annals of Operations Research*, vol. 223, no. 1, pp. 81–93, 2014.

[8] A. K. Naimzada and F. Tramontana, "Dynamic properties of a Cournot-Bertrand duopoly game with differentiated products," *Economic Modelling*, vol. 29, no. 4, pp. 1436–1439, 2012.

[9] J. Ma, L. Sun, S. Hou, and X. Zhan, "Complexity study on the Cournot-Bertrand mixed duopoly game model with market share preference," *Chaos*, vol. 28, no. 2, pp. 023101–023110, 2018.

[10] S. S. Askar, "On complex dynamics of cournot-bertrand game with asymmetric market information," *Applied Mathematics and Computation*, vol. 393, Article ID 125823, 2021.

[11] S. S. Askar and M. F. Elettreby, "The impact of cost uncertainty on Cournot oligopoly games," *Applied Mathematics and Computation*, vol. 312, pp. 169–176, 2017.

[12] S. S. Askar, M. F. El-Wakeel, and M. A. Alrodaini, "Exploration of complex dynamics for cournot oligopoly game with differentiated products," *Complexity*, vol. 2018, Article ID 6526794, 13 pages, 2018.
[13] S. S. Askar, "The impact of cost uncertainty on Cournot duopoly game with concave demand function," *Journal of Applied Mathematics*, vol. 2013, Article ID 809795, 5 pages, 2013.
[14] S. S. Askar, "A competition of duopoly game whose players are public: dynamic investigations," *Communications in Nonlinear Science and Numerical Simulation*, vol. 111, Article ID 106486, 2022.
[15] H. M. Wang and J. Ma, "Complexity analysis of a cournot-bertrand duopoly game model with limited information," *Discrete Dynamics in Nature and Society*, vol. 2013, Article ID 287371, 6 pages, 2013.
[16] M. Ueda, "Effect of information asymmetry in Cournot duopoly game with bounded rationality," *Applied Mathematics and Computation*, vol. 362, Article ID 124535, 2019.
[17] T. Puu, "Chaos in duopoly pricing," *Chaos, Solitons and Fractals*, vol. 1, no. 6, pp. 573–581, 1991.
[18] A. A. Elsadany, "Dynamics of a Cournot duopoly game with bounded rationality based on relative profit maximization," *Applied Mathematics and Computation*, vol. 294, pp. 253–263, 2017.
[19] A. M. Awad, S. S. Askar, and A. A. Elsadany, "Complex dynamics investigations of a mixed Bertrand duopoly game: synchronization and global analysis," *Nonlinear Dynamics*, vol. 107, no. 4, pp. 3983–3999, 2022.
[20] W. Zhou and H. Li, "Complex dynamical behaviors in a Bertrand game with service factor and differentiated products," *Nonlinear Dynamics*, vol. 106, no. 3, pp. 2739–2759, 2021.
[21] S. Brianzoni, L. Gori, and E. Michetti, "Dynamics of a Bertrand duopoly with differentiated products and nonlinear costs: analysis, comparisons and new evidences," *Chaos, Solitons and Fractals*, vol. 79, pp. 191–203, 2015.
[22] Z. Wei, W. Tan, A. A. Elsadany, and I. Moroz, "Complexity and chaos control in a Cournot duopoly model based on bounded rationality and relative profit maximization," *Nonlinear Dynamics*, vol. 111, no. 18, pp. 17561–17589, 2023.
[23] G. Sarafopoulos and K. Papadopoulos, "Complexity and chaos control of A cournot duopoly game with relative profit maximization and heterogeneous expectations," *KnE Social Sciences*, vol. 8, no. 1, pp. 172–193, 2023.
[24] D. Rand, "Exotic phenomena in games and duopoly models," *Journal of Mathematical Economics*, vol. 5, no. 2, pp. 173–184, 1978.
[25] G. I. Bischi, L. Stefanini, and L. Gardini, "Synchronization, intermittency and critical curves in a duopoly game," *Mathematics and Computers in Simulation*, vol. 44, no. 6, pp. 559–585, 1998.
[26] J. Tanimoto, *Evolutionary Games with Sociophysics*, Springer, Berlin, Germany, 2019.
[27] L. Fanti, L. Gori, and M. Sodini, "Nonlinear dynamics in a Cournot duopoly with isoelastic demand," *Mathematics and Computers in Simulation*, vol. 108, pp. 129–143, 2015.
[28] Y. Peng and Q. Lu, "Complex dynamics analysis for a duopoly Stackelberg game model with bounded rationality," *Applied Mathematics and Computation*, vol. 271, pp. 259–268, 2015.
[29] A. Kuznetsov and A. G. F. Meijer, *Numerical Bifurcation Analysis of Maps: From Theory to Software*, Cambridge University Press, Cambridge, UK, 2019.